Journal of Energy Technology and Environment

Journal homepage: www.nipesjournals.org.ng

NIPES

Modelling and Simulation of a Four Wheel Plugged in Electric Vehicle (PEV)

M. I. Faruk[a], E. C. Anene[b], J. D. Jiya[c]
"aDepartment of Physics Bayero University Kano, Nigeria."
"bcDepartment of Electrical and Electronics Engineering, Abubakar Tafawa Balewa University Bauchi, Nigeria."

ARTICLE INFORMATION

ABSTRACT

Electric vehicles (EVs) are becoming promising alternative energy sources to be the remedy for the challenging environmental problems (greenhouse emissions, air pollution and petrol dependency) and sustainable transport systems. Pure or Plugged-in electric vehicles (PEVs) use batteries to store the energy that will be transformed into mechanical power by electric motor(s) only, i. e., internal combustion engine (ICE) is not present. Pure electric vehicles may adopt two (or four) in-wheel motors in their powertrains. In this case, every motor is driven by a dedicated power converter that must control wheel's speed and torque. As expected, the simplification of the mechanical design is attained at the expense of increased complexity of the power electronics and controllers. This research therefore focus on the mathematical modelling of the four wheel plugged-in electric vehicle. The mathematical modelling is obtained through hard modelling methods. The dynamic model simulation is carried out and then verified using a computer aided computer software design (CACSD) i.e. the Simulink block diagram interface in the MATLAB development environment. The resulting output will significantly provide an in depth performance/behavior of the system, and consequently give an avenue for system performance control and optimization.

1. Introduction

Conventional vehicles which use only internal combustion engines (ICE) have experienced and enjoyed monopoly for almost a century as power sources of road transport vehicles [1]**.** They have experienced continuous development in manufacturing technology, materials science, vehicle control, driver comfort, excellent performance and advanced security, for relatively low prices [2]. Today internal combustion engines are at their mature levels that any further development to increase engine efficiency and minimize the emissions is expected to be very little. Any improvement in engine and fuel technology for better efficiency and emissions either increase the cost to uncompetitive levels or bring additional environmental problems when especially considering life cycle of the engines and fuels. This means that despite the struggles by industry and academia to improve ICE efficiency, their output still continue to be on the low side. Figure 1 (Soylu, 2011) shows that approximately only 30% of the energy produced in the ICE combustion reaction is converted into mechanical power. This means that, approximately 70% of the energy liberated by combustion is lost. The wasted energy of the ICEs is transformed into exhaust gases.

These exhaust gases are a mixture formed by carbon dioxide (CO_2) and, to a lower extent, nitrogen oxides (NOx), hydrocarbons (CxHy), carbon monoxide (CO) and soot. Carbon dioxide is known to block the earth's radiation emissions back into the outer space thus promoting global temperature rise (the greenhouse effect).
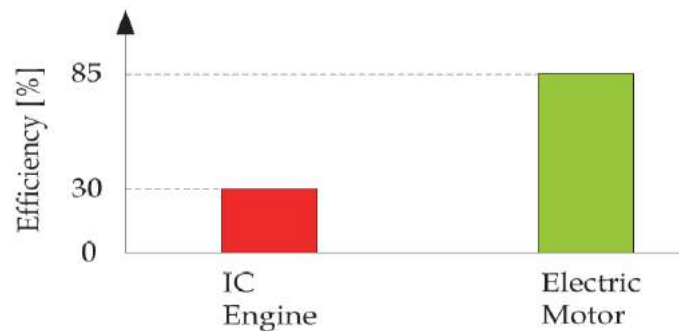

Figure 1: Internal Combustion Engine and Electric Motor Efficiency [2]

The effect of these gases researchers say, is silently creating other global catastrophic changes like sea level rise, air pollution in big cities, respiratory system diseases including lung cancer.

Figure 1 shows clearly that the efficiency of electric motors for EVs are far superior to ICE and could do an excellent job in propulsion of vehicles, helping to solve the serious climate, air pollution and noise problems created by ICEVs. Additionally, an electric vehicle can convert the vehicle's kinetic energy to electrical energy and store it during braking and coasting. All these benefits of electric vehicles are starting to justify, a century later, attention of industry, academia and policy makers again as promising alternatives for urban transport [3]. Furthermore, optimizing and conserving energy is a large focus of society today. This is largely due to a predicted energy shortage if global consumption continues on its current trajectory [4]. Many ways of saving energy therefore have been researched and implemented to this point, such as super-efficient windows for large buildings, lights bulbs that last years and use minimal electricity as well as smarter manufacturing technologies such as optimizing blast furnace operation [5]. Some of the most significant efforts in energy saving however, have been put into the area of industrial and personal transportation. The large majority of vehicles still run on fossil fuels, but an increasing amount of research has been put into developing and optimizing alternative energy sources such as electric, biofuels, natural gas, and even solar power for transportation. Hybrid electric vehicles (HEVs) attempt to mate the utility of a gasoline/diesel engine with the environmentally friendly characteristics of an electric drive. HEV technologies provide a fuel economy improvement and enable HEVs to exhaust less emissions compared to the conventional internal combustion engine vehicles (ICEVs), but HEVs cannot completely resolve the above mentioned issues. Thus, HEVs are only a temporary step in the development from ICEVs to pure/plugged-in electric vehicles (PEVs) [4]. Electric vehicles (EVs) are therefore becoming promising alternatives to be the remedy for the challenging problems and sustainable transport as they can use centrally generated electricity as a power source. EVs are of various types, but the plugged-in types of EVs are made up of an electric motor incorporated into the center of a wheel which drives it directly. The wheels contain not only the braking components, but also all of the functionalities that were formerly performed by the ICE. The motor is installed close to the drive wheel, and moves the wheel through extremely small drive shaft.
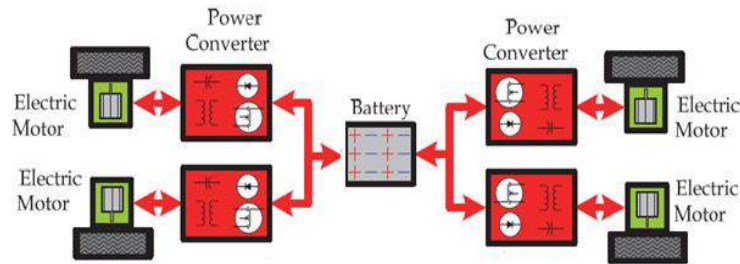
Figure 2: Four- Motor Plugged-In Electric Vehicle

The motor applies torque directly to the wheel, and it is only linked via electrical connections that converge to a central controller hub. Such a configuration results in over-actuation, (*which causes* instability in driving around corners or even in a straight line), difficulties in **speed** and **torque** control which therefore results in more optimization potential. The PEV presented in this research comprises of four (4) permanent-magnet brushless direct-current (BLDC) electric motor used as the in-wheel electric motors. Most of the control effort up to this point has been put toward the area of speed, safety, stability and range control [4]. Therefore, various control strategies such as road-friction estimation [6], a system of electric differentials [7], PID state space technique for the speed cruise control system by [8] as well as a fuzzy gain scheduling PI speed control for EVs and ICEVs [9], have been investigated in order to provide a comprehensive mechanism for accurately driving these EVs.

2. Methodology

2.1 Mathematical Modelling

The representation of a system either mechanistic or empirical is the key in building a reliable control system. The plugged-in EV model will describe the dynamics of the system which will aid significantly in developing an effective visual representation and subsequently the development of an operational control algorithm. Therefore to develop the empirical model for the four-wheel EV its mathematical dynamics is required. The mathematical representations were obtained as described in Equations 1 to 30 [10, 11, 12, 13]. There are several variables used for the four-wheel model, and are as shown in Table 1. The mathematical equations cover longitudinal dynamics from wind resistance and from climbing a hill, the four wheel dynamics as well as the in-wheel motor dynamics.

2.2 Vehicle Aerodynamics

Vehicle aerodynamics are important to include in a complete model. The effect of air resistance on a vehicle is proportional to the area of the vehicle that pushes through the air, the density of the air, a drag coefficient, and the velocity squared of the vehicle.

$$F_{drag} = \frac{1}{2}\rho A C_D V^2 \tag{1}$$

There are different values for the drag coefficient and area of a vehicle depending on the shape and size of the car. For a medium to large vehicle, typical values for the drag coefficient range from 0.30 to 0.42 and area that ranges from 1.90 to 2.16 square meters. Here, a median value of 0.36 will be used for the drag coefficient and 2.03 square meters will be used for the area. The density of air will vary depending on the elevation, humidity, and temperature. Here a value of 1.225 kilograms per meter cubed will be used. This corresponds to a temperature of fifteen degrees Celsius and a pressure of 101.32 kilo-Pascal [12].

2.3 Longitudinal Dynamics

Longitudinal dynamics also affect the forces on the tires of a vehicle as in Figure 3, a vehicle moving up an inclined surface. The forces on the front and rear wheels can be found by taking the sum of the forces in the z-direction and the sum of the moments in the y-direction as in equations 2 and 3. The friction forces on the front and rear tires are approximated by the normal force on the tires times a coefficient of friction.
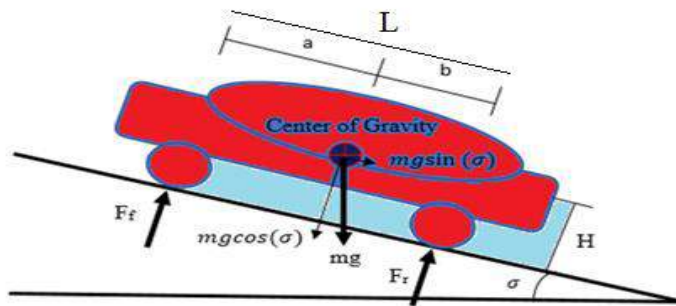

Figure 3: Vehicle Dynamics

$$\Sigma F_z = 0: F_f + F_r(-\sigma) = 0 \tag{2}$$

$$\Sigma M_{y-axis} = 0: F_f\mu H + F_r\mu H + F_r b - F_f a = 0 \tag{3}$$

Solving equations 2 and 3 gives equations for the front and rear forces as shown in equations 4 and 5

$$F_r = \frac{amgcos(\sigma) - \mu Hmgcos(\sigma)}{L} \tag{4}$$

$$F_r = \frac{\mu Hmgcos(\sigma) + bmgcos(\sigma)}{L} \tag{5}$$

The values of coefficients of friction will vary depending on road conditions, but as a conventional estimate of rubber to concrete interaction, a value of 0.8 will be used**.**

It should be noted that the height of the center of gravity from the ground must be accounted for, which can be determined experimentally by using a car trailer to provide an inclined surface, placed on scales. This will shift the weight on the front and rear tires, using Equations 2 and 3 to determine the height of the center of gravity. Therefore the vehicle will have to be constrained physically so that is does not roll off of the trailer. This means that the friction forces are no longer keeping the vehicle in place, and they will be ignored when doing calculations

2.4 Four-Wheel Mathematical Dynamics

The four-wheel model is relatively complex because it involves slip angles and the forces on the four tires as in Figure 4
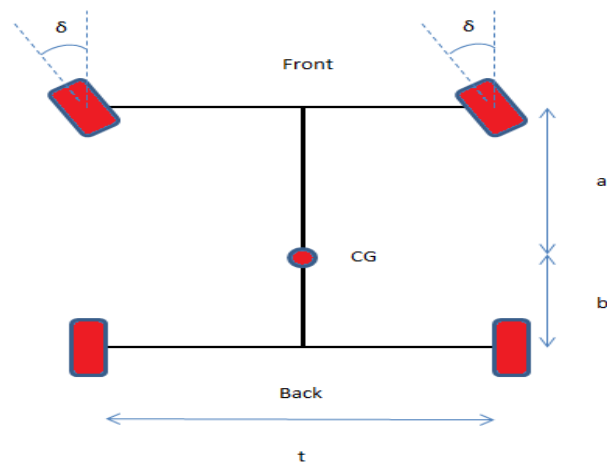

Figure 4: Four Wheel Vehicle Diagram

From Figure 4, it can be noted that both front wheels have an applied steering angle δ. The width of the car is designated by t, a and b are the lengths from the front and rear to the center of gravity. The forces on the tires that propel the vehicle forward are modeled as perpendicular to the tire length and width as shown in Figure 5. The forces shown in Figure 5 can be resolved into vectors pointing in the x- and y-directions as shown in Figure 6. Figure 6 can be used to write the equations of motion.
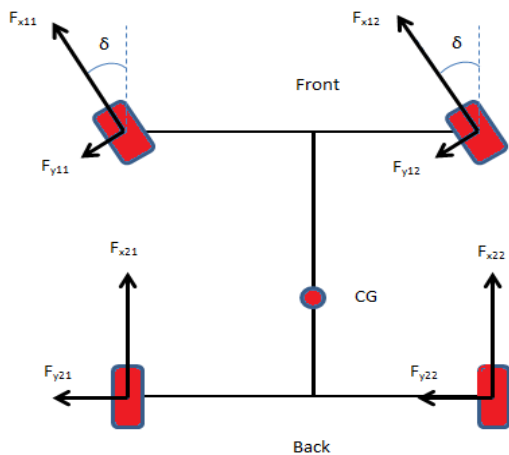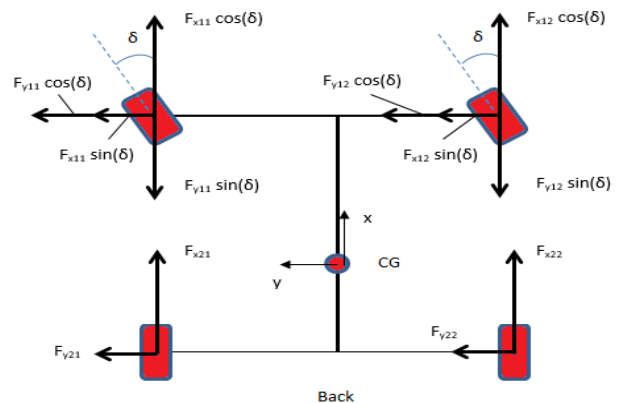

Figure 5: Four Wheel Force Diagram

Figure 6: Four-Wheel Force Resolution Diagram

The sum of the moments, sum of the lateral forces, and sum of the longitudinal forces are shown in Equations 6, 7, and 8.

$$\Sigma M_z: I\dot{r} = (F_{x12}cos\delta)\frac{t}{2} - (F_{y12}sin\delta)\frac{t}{2} + (F_{x12}sin\delta)a$$
$$+ (F_{y12}cos\delta)a + (F_{y11}cos\delta)a + (F_{x11}sin\delta)a -$$
$$(F_{x11}cos\delta)\frac{t}{2} + (F_{y11}sin\delta)\frac{t}{2} - F_{x21}\frac{t}{2} - F_{y21}b - F_{y22}b$$
$$+ F_{x22}\frac{t}{2}$$

(6)

$$\Sigma F_y: (F_{y21}+F_{y22}) + (F_{y11}+F_{y12}) + (F_{x11}+ F_{x12}) =$$
$$m(\dot{U}+Vr)$$

(7)

$$\Sigma F_x: F_{x21} + F_{x22} + (F_{x11}+ F_{x12}) - (F_{y11} + F_{y12})$$
$$- \frac{1}{2}\rho C_d A V^2 = m(\dot{V}-Ur)$$

(8)

The tire forces in Equations 6, 7, and 8 can be written in terms of the tire slip angles. The diagram of the tire slip angles is as shown in Figure 7 and a diagram showing the velocity vector resolution at each tire is shown in Figure 8. The velocity vector resolution shown in Figure 8 is used to write the slip angles as in Equations 9, 10, 11, and 12.

$$tan(\delta+\alpha_{11}) = \frac{U+ra}{V-r\left(\frac{t}{2}\right)}$$

(9)

$$tan(\delta+\alpha_{12}) = \frac{U+ra}{V+r\left(\frac{t}{2}\right)}$$

(10)

(11)

$$tan(\alpha_{21}) = \frac{U+rb}{V-r\left(\frac{t}{2}\right)}$$

$$tan(\alpha_{22}) = \frac{U+rb}{V+r\left(\frac{t}{2}\right)}$$
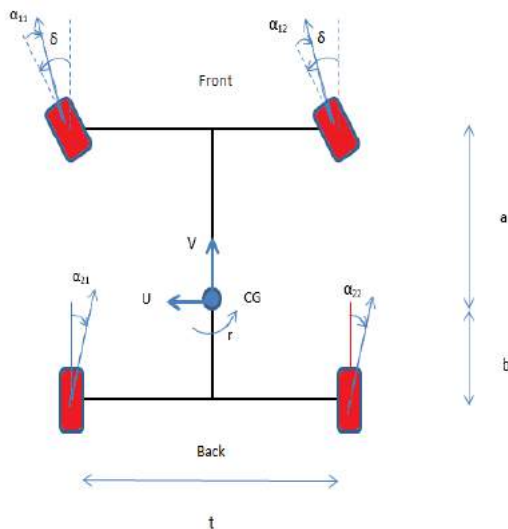
(12)
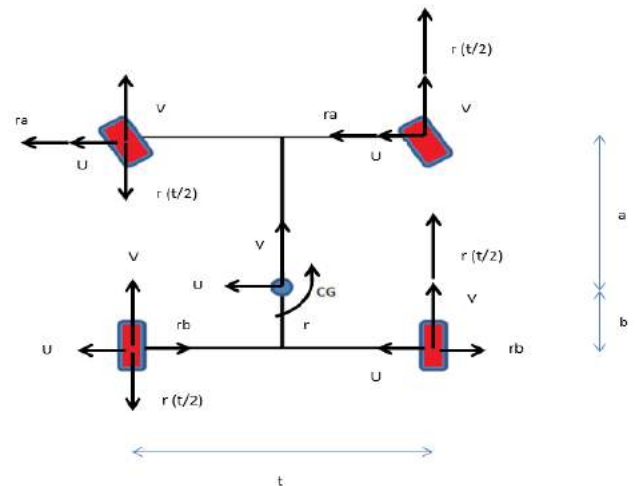

Figure 7: Slip angle Diagram   Figure 8: Four Wheel Velocity Vector Diagram

Equations 6 through 12 can be linearized assuming small angles. Linearized equations for the sum of the moments in the z-direction, sum of the forces in the y-direction, and sum of the forces in the x-direction are shown in Equations 13, 14, and 15.

$$\Sigma M_z : I\dot{r} = (F_{x12})\frac{t}{2}(\delta F_{y12})\frac{t}{2} + (\delta F_{x12}) + (F_{y12}) +$$
$$(F_{y11}) + (\delta F_{x11}) - (F_{x11})\frac{t}{2} + (\delta F_{y11})\frac{t}{2} - F_{x21}\frac{t}{2} -$$
$$F_{y21}b - F_{y22}b + F_{x22}\frac{t}{2} \tag{13}$$

$$\Sigma F_y : (F_{y21} + F_{y22}) + (F_{y11}+F_{y12}) + (F_{x11} + F_{x12}) =$$
$$m(\dot{U} + Vr) \tag{14}$$

$$\Sigma F_x : F_{x21} + F_{x22} + F_{x11} + F_{x12} - (F_{y11}+F_{y12}) - \frac{1}{2}\rho C_d A V^2 =$$
$$(\dot{V} - Ur) \tag{15}$$

Each rear tire will be driven by applying a torque to the wheels. This is modeled using Equations 16 and 17.

$$I_w\dot{\omega}_{21} = T_{21} - RF_{x21} \tag{16}$$

$$I_w\dot{\omega}_{22} = T_{22} - RF_{x22} \tag{17}$$

The moment of inertia of the tires is assumed to be small, then the rear tire force created by a torque input can be simplified as in Equations 18 and 19.

$$F_{x21} = \frac{T_{21}}{R} \tag{18}$$

$$F_{x22} = \frac{T_{22}}{R} \tag{19}$$

The slip angles of the tires can be linearized as in Equations 20 through 23.

$$\alpha_{11} = \frac{U+ra}{V - r\left(\frac{t}{2}\right)} - \delta \tag{20}$$

$$\alpha_{12} = \frac{U+ra}{V + r\left(\frac{t}{2}\right)} - \delta \tag{21}$$

$$\alpha_{21} = \frac{U-br}{V - r\left(\frac{t}{2}\right)} \tag{22}$$

$$\alpha_{22} = \frac{U-br}{V + r\left(\frac{t}{2}\right)} \tag{23}$$

The normal forces on both of the front and rear tires is presented in Equations 14 and 15. Therefore the friction force on each individual tire will oppose motion and will be proportional to the coefficient of friction times the normal force on the vehicle. The sign of the friction force can be calculated by dividing the longitudinal speed of the vehicle by the magnitude of the longitudinal speed and multiplying by a negative sign. Equations 24 through 27 represents the individual forces on each tire due to friction.

$$Friction_{x11} = -\mu\frac{V}{|V|}\left(\frac{\mu Hmgcos(\sigma)+bmgcos(\sigma)}{2L}\right) \tag{24}$$

$$Friction_{x12} = -\mu\frac{V}{|V|}\left(\frac{\mu Hmgcos(\sigma)+bmgcos(\sigma)}{2L}\right) \tag{25}$$

$$Friction_{x21} = -\mu\frac{V}{|V|}\left(\frac{amgcos(\sigma)-\mu Hmgcos(\sigma)}{2L}\right) \tag{26}$$

$$Friction_{x22} = -\mu\frac{V}{|V|}\left(\frac{amgcos(\sigma)-\mu Hmgcos(\sigma)}{2L}\right) \tag{27}$$

The friction forces and the slip angles are then substituted into the Equations of motion as shown in Equation 28, 29, and 30.

$$\Sigma M_z: I\dot{r} = (Friction_{x12})\frac{t}{2} - \delta(C_{af}\alpha 12)\frac{t}{2} + \tag{28}$$
$$\delta(Friction_{x12})a + (C_{af}\alpha 12)a + (C_{af}\alpha 11)a +$$
$$\delta(Friction_{x11})a - (Friction_{x11})\frac{t}{2} + \delta(C_{af}\alpha 11)\frac{t}{2} -$$
$$(Friction_{x21} + \frac{T_{21}}{R})\frac{t}{2} - C_{ar}\alpha 21 b - C_{ar}\alpha 22 b +$$
$$(Friction_{x22} + \frac{T_{22}}{R})\frac{t}{2}$$

$$\Sigma F_y: (C_{ar}\alpha 21 + C_{ar}\alpha 22) + (C_{af}\alpha 11 + C_{af}\alpha 12) + \tag{29}$$
$$(Friction_{x11} + Friction_{x12}) = (\dot{U} + Vr)$$

$$\Sigma F_x: Friction_{x21} + \frac{T_{21}}{R} + Friction_{x22} + \frac{T_{22}}{R} + Friction_{x11} \tag{30}$$
$$+ Friction_{x12} - \delta C_{af}(\alpha 11 + \alpha 12) - \frac{1}{2}\rho C_d AV^2 = (\dot{V} - Ur)$$

Therefore, these equations of motion will be used to model the system behavior in time using MatLab/Simulink development environment which will be used to determine the transient response/ performance of the vehicle when subjected to different arbitrary input.

3. Results and Discussion

Table 1: Simulation Parameters

S/N	Term	Symbol	Value
1	Torque applied to left rear wheel	T_{21}	500Nm
2	Torque applied to right rear wheel	T_{22}	500Nm
3	Longitudinal coefficient of friction	μ	0.8
4	Front left slip angle	α_{11}	0.9
5	Front right slip angle	α_{12}	0.8
6	Rear left slip angle	α_{21}	1.0

7	Rear right slip angle	α_{22}	1.0
9	Front Area	A	2.03m^2
10	Drag Coefficient	C_d	0.36
11	Air Density	ρ	1.225kg/m^3
12	Steering Angle	δ	0.1
13	Length of wheelbase	L	2.77m
14	Distance from front of car to center of gravity	a	1.51m
15	Distance from rear of car to center of gravity	b	1.26m
16	Radius of path curvature	R	0.29m
17	Angle of rotation	Θ	0
18	Force of gravity	CG	9.81ms
19	Damping coefficient	B	0.22vrad^{-1}
10	Rotor inertia	J	1.74 x 10^3
11	Torque constant	Kτ	0.02Nm

3.1 Simulation

A Simulink block diagram was developed based on Equations (28), (29) and (30). Figures 9 and 10 shows the Simulink block diagram of the PEV. While Figure 11 shows the arbitrary input used to excite the system so as to study the response of the model to inputs and initial conditions in relation to rotational speed. Table 1 shows the system parameters and values used in this work.
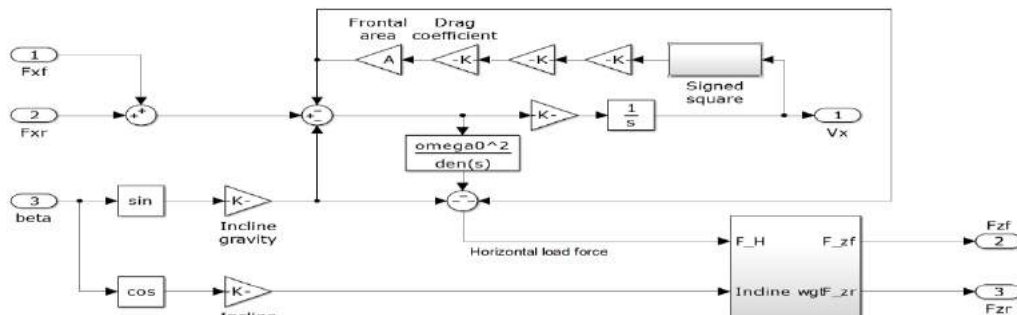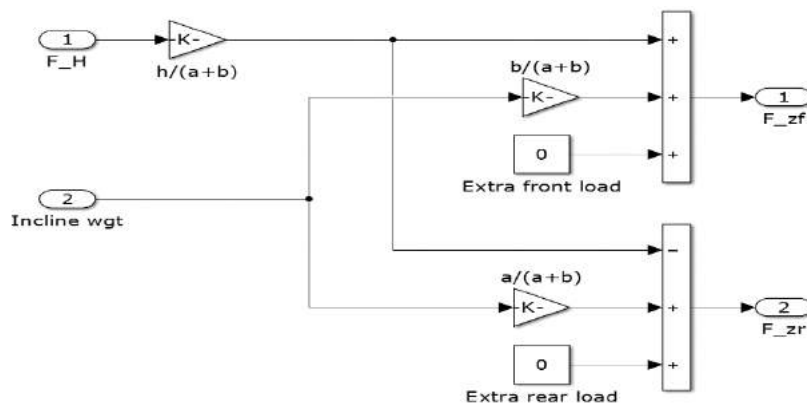

Figure 9. Vehicle Dynamics
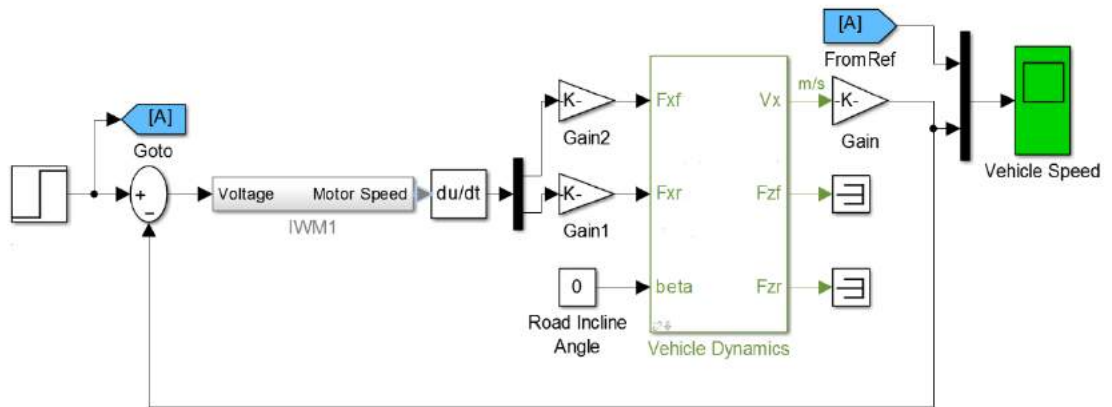

Figure 10. Load Transfer

Figure 11.Arbitrary Input Excited Simulink Model to Test Rotational Speed

Therefore with the model subjected to various signals from the signal generator representing different driving conditions, it can be observed Figure 12 depict the PEV simulated model output transient response performance/behavior when subjected to a step input signal. Furthermore from the output response it can be ascertained that, while a reference step time (blue line) of five seconds and a final rotational speed of five rads/sec was set, the model response (green line) shows an initial tracking of the reference signal up till the five (5) seconds position and then rise continuously with no steady state attainment.

It can be further observed from Figures 13 to 16, as the PEV simulated model were subjected to different arbitrary input exciting signals representing different driving conditions, and there corresponding transient response performance were also obtained. Whereby the output responses from the different inputs set shows consistency in initial or close tracking of the input references. These output responses verified the validity of the simulated PEV model and gives an avenue for model observations and the subsequent controller design as well as other control techniques design possibilities. This is because the output performances clearly shows poor tracking of the input/reference signals.
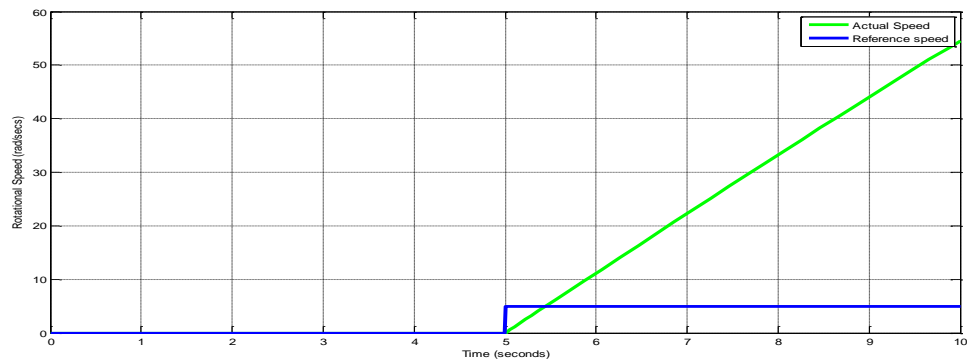

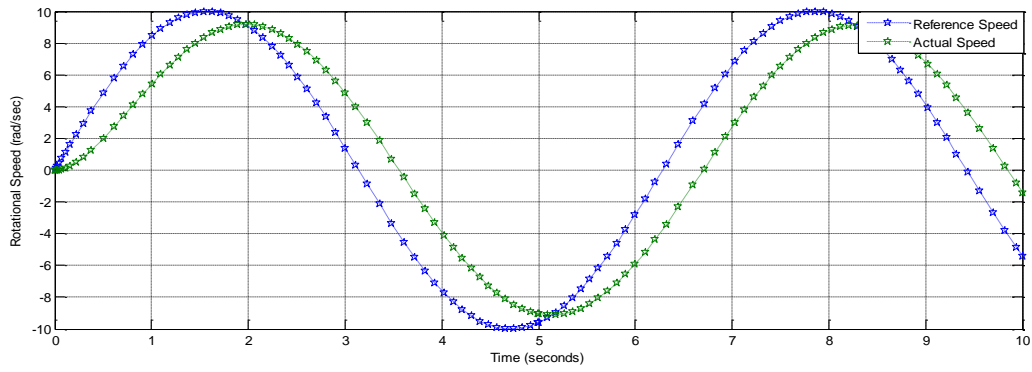**Figure 12. PEV Model Step Input Response**

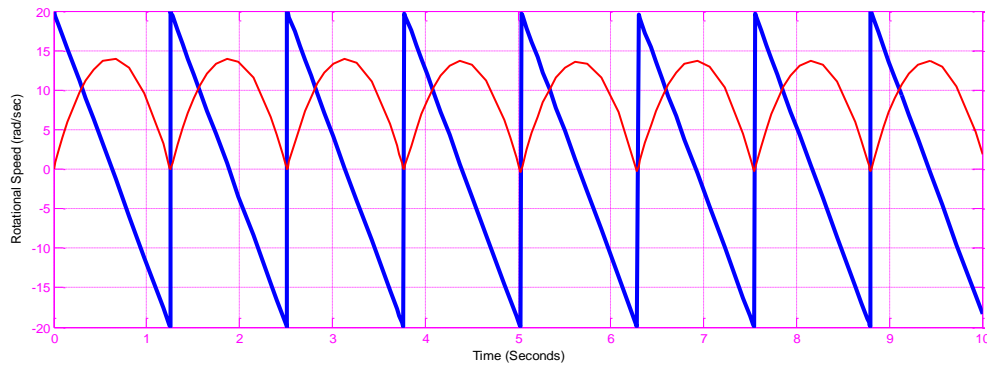**Figure 13. PEV Model Sinousidal Input Response**

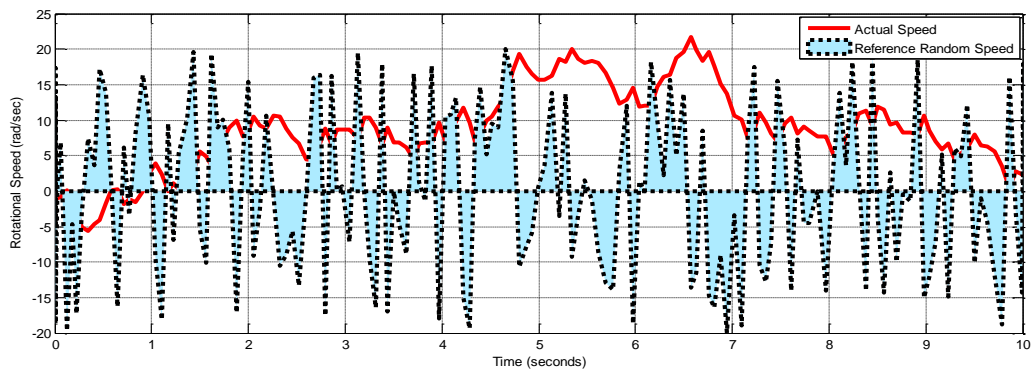**Figure 14. PEV Model Sawtooth Input Response**

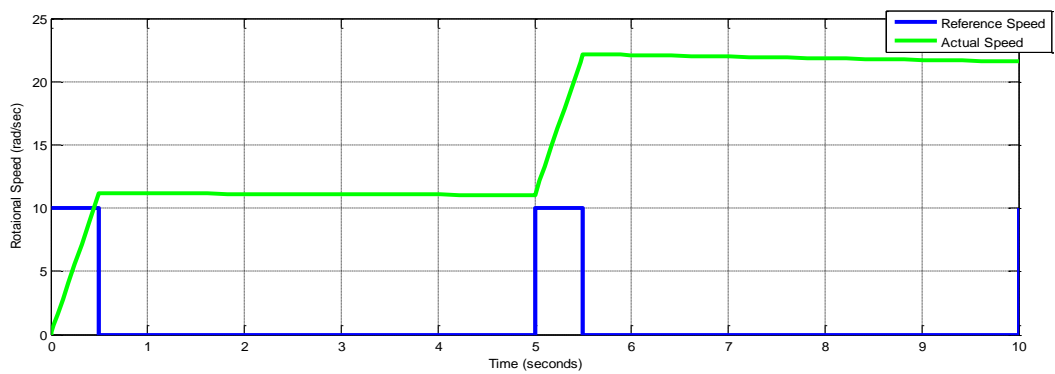**Figure 15**. **PEV Model Random Signal Input Response**

Figure 16: **PEV Model Square wave Input Response**

Moreover the validity of the fully synchronized PEV model can be ascertained by Schwartz *et al* [14]. In their research the modelling aspect focused on the steering dynamics, tire dynamics and horizontal dynamics in Matlab/Simulink development environment. Ignoring the in-wheel dynamics as well as the vehicle aero dynamics. [15] Used Matlab/Simulink to model and develop a model predictive control Allocation in electric vehicle drive trains. The modelling in [15] used induction motors as the front in-wheel motors and permanent magnet motors for the rear wheel motors. Hence the output response performances in Figures 12-16 shows some level of concurrence with [14] and [15] with slight difference due to minor differences in the mathematical models used.

4. Conclusion

The dynamic model of the plugged-in electric vehicle system were obtained and successfully represented in Matlab/Simulink development interface. The transient outputs response performances from the arbitrary inputs clearly gives a pictorial view of the PEV system performance with respect to the EV rotational speed movement. This pave way for various parameter (speed, torque and energy consumption) performance analysis and improvement (controller design) capabilities.

Nomenclature

$\dot{V}$	Change in velocity
m	Mass
U	Initial velocity
μ	Longitudinal coefficient of friction
Σ	acceleration due to gravity
w	half of the track width
H	Height to center of gravity
L	Total length of vehilcle
Mf	Mass of front axle
Mr	Mass of rear axle
ρ	Density of air
rtire	Radius of titr
Fr	Force on ear tire
Ff	Force on front tire
δ	Steering angle
α	Slip angle

References

[1]   Z. Jian, W. Xuhui, and Z. Lili, "Research of Parameter Self-learning Fuzzy Control Strategy in motor control system for Electric Vehicles," IEEE Trans. Sys. Man, Cybern, no. 5, pp. 111–115, 2013.
[2]   S. Soylu, "Electric Vehicles-The Benefits and Barriers Edited," 2011.
[3]   N. Benalie, W. Pananurak, S. Thanok, and M. Parnichkun, "Improvement of adaptive cruise control system based on speed characteristics and time headway," 2009 IEEE/RSJ Int. Conf. Intell. Robot. Syst., pp. 2403–2408, Oct. 2009.
[4]   Z. Li, A. Khajepour, and J. Song, "A comprehensive review of the key technologies for pure electric vehicles," Elsevier, Energy, vol. 182, pp. 824–839, 2019.
[5]   C. Zhou and J. R. Vehec, "Optimizing Blast Furnace Operation to Increase Efficiency and Lower Costs," Industial Technology Program, U.S Department of Energy, Efficiency and Renewable Energy, 2014. .
[6]   J. Wang and Y. Chen, "Adaptive Vehicle Speed Control With Input Injections for Longitudinal Motion Independent Road Frictional Condition Esitmation," IEEE Trans. Veh. Technol., pp. 839–848, 2011.
[7]   Y. C. and J. Wang, "Design and Evaluation on Electric Differentials for Overactuated Electric Ground Vehicles With Four Independent In-Wheel Motors," IEEE Trans. Veh. Technol., pp. 1534–1542, 2012.
[8]   H. Balaska, S. Ladaci, and H. Schulte, "Adaptive Cruise Control System for an Electric Vehicle Using a Fractional Order Model Reference Adaptive Strategy," Int. Fed. Autom. Control. Elsevier, pp. 194–199, 2019.

[9]   F. U. Syed, M. L. Kuang, M. Smith, S. Okubo, and H. Ying, "Fuzzy Gain-Scheduling Proportional – Integral Control for Improving Engine Power and Speed Behavior in a Hybrid Electric Vehicle," IEEE Trans. Veh. Technol., vol. 58, no. 1, pp. 69–84, 2009.

[10]   D. Mikle and B. Martin, "Torque Vectoring for an Electric All-wheel Drive Vehicle Torque Vectoring for an Electric Vectoring for for an an Electric Electric All-wheel Vehicle," IFAC Pap. icle Dyn. Int. Fed. Autom. Control Hosting by Elsivier, vol. 27, pp. 163–169, 2019.

[11]   J. Hong, Z. Wang, T. Zhang, and H. Yin, "Research on Performance Simulation of Load Isolation Pure Electric Driving Vehicles," vol. 104, pp. 544–549, 2016.

[12]   R. N. Jazar, Vehicle Dynamics, Theory and Application. Springer, 2017.

[22]   R. Martino, "Modellling and simulation of the Dynamics Behavior of Automobile," J. Univ. Houte Alsace-mule House, pp. 512–518, 2005.

[13]   H. Sakai, "Theoretical and Experimental Studies on the Dynamic Properties of Tyres Part 1: Review of Theories of Rubber Friction," Int. J. Veh. Des., vol. 2, no. 1, pp. 78–110, 1981.

[14]   M.Schwartz, F. Siebnrock, S. Hohmann, "Model Predictive Control Allocation of an Over-actuated Electric Vehicle with Single Wheel Actuator," International Federation of Automatic Control, pp. 162–169, 2019.

[15]   T. Bachle, K. Granchen, M. Buchholz, K. Dietmayer, "Model Predictive Control Allocation in Electric Vehicle Drive Trains," International Federation of Automatic Control, pp. 335–340, 2015

Appendix
Matlab Codes

```
function four_wheel_model
%Constants
m = 1724; % mass
Cd = 0.36; % coefficient of drag
A = 2.03; % car frontal area
g = 9.81; % acceleration due to gravity
sigma = 0.2; % grade
a = 1.51; % distance from center of mass to front axle
b = 1.26; % distance from center of mass to rear axle
c = 1.92; % track width;
w = 0.5*c; % half of the track width
H = 0.6; %height to center of gravity
L = a+b; % total length of the vehicle
mf = m * b / L; % mass on front axle
mr = m * a / L; % mass on rear axle
Cyr = 0.19*(mr)*g*(180/pi); % cornering stiffness rear tires (N/rad)
Cyf = 0.19*(mf)*g*(180/pi); % cornering stiffness front tires (N/rad)
rho = 1.225; % density of air
rtire = 0.29; % radius of tire (m)
mu = 0.8; % coefficient of friction
T21 = 500; % Torque to left rear tire (Nm)
T22 = 500; % Torque to right rear tire (Nm)
delta = 0.1; % Desired steering angle
q0 = [0;0;0;0;0;0;0;0]; % initial state
T = linspace(0,1,2000); % solution time mesh
[~,q] = ode45(@cartv, T, q0);
%x
figure(1)
subplot(4,2,1);
plot(T, q(:,1));
xlabel('time');
ylabel('rotational speed');
title('State Variables');
% xdot
subplot(4,2,2); plot(T, q(:,4)); xlabel('time'); ylabel('rotational speed');
steering = zeros(N,1);
```

```
slip11 = zeros(N,1);
slip12 = zeros(N,1);
slip21 = zeros(N,1);
slip22 = zeros(N,1);
ay = zeros(N,1);
ax = zeros(N,1);
for i = 1:N
% State variables
%x = q(i,1); % body fixed x-axis
%y = q(i,2); % body fixed y-axis
%s = q(i,3); % body yaw angle (psi)
xd = q(i,4); % body fixed x-axis velocity
yd = q(i,5); % body fixed y-axis velocity
sd = q(i,6); % body yaw rate (psi_dot)
%xx = q(i,7); % global x position of car center of mass
%yy = q(i,8); % global y position of car center of mass
% Drag force
axd = abs(xd);
fdrag = 0.5*rho*Cd*A*xd*axd; 120

% Tire slip angle
ad = xd - w*sd;
abs_ad = abs(ad);
alpha11 = 0;
if abs_ad > 0
alpha11 = atan((yd + a*sd)/ad) - delta;
end
alpha21 = 0;
if abs_ad > 0
alpha21 =atan((yd - b*sd)/ad);
end
af = xd + w*sd;
abs_af = abs(af);
alpha12 = 0;
if abs_af > 0
alpha12 = atan((yd + a*sd)/af) - delta;
end
alpha22 = 0;
if abs_af > 0
alpha22 = atan((yd - b*sd)/af); 121

end
% Tire forces
f11grade = 0;
if axd > 0
f11grade = -(mu*xd/axd)*(mu*H*m*g*cos(sigma) + b*m*g*cos(sigma))/(2*L);
end
f11x = -f11grade;
f11y = -Cyf*alpha11;
f21grade = 0;
if axd > 0
f21grade = -(mu*xd/axd)*(a*m*g*cos(sigma) - mu*H*m*g*cos(sigma))/(2*L);
end
f21x = -f21grade + T21/rtire;
f21y = -Cyr*alpha21;
f12grade = 0;
if axd > 0
f12grade = -(mu*xd/axd)*(mu*H*m*g*cos(sigma) + b*m*g*cos(sigma))/(2*L);
end
f12x = -f12grade;
```

127

```
f12y = -Cyf*alpha12; 122

f22grade = 0;
if axd > 0
f22grade = -(mu*xd/axd)*(a*m*g*cos(sigma) - mu*H*m*g*cos(sigma))/(2*L);
end
f22x = -f22grade + T22/rtire;
f22y = -Cyr*alpha22;
steering(i) = delta;
slip11(i) = alpha11*180/pi;
slip12(i) = alpha12*180/pi;
slip21(i) = alpha21*180/pi;
slip22(i) = alpha22*180/pi;
ay(i) = (-xd*sd + ( f11x*sin(delta) +f12x*sin(delta) + f11y*cos(delta) + f21y + f12y*cos(delta) + f22y )/m);
ax(i) = (f21x + f22x + f11x*cos(delta) + f12x*cos(delta) - sin(delta)*(f11y + f12y)- fdrag + sd*yd)/m;
end
%-----------------------------------------------------------------------
figure(4);
title('Derived Parameters from State Variables'); 123
% assumes: linear cornering force proportional to tire slip angle
function qdot = cartv(~,q)
% State variables
%x = q(1,:); % body fixed x-axis
%y = q(2,:); % body fixed y-axis
s = q(3,:); % body yaw angle (psi)
xd = q(4,:); % body fixed x-axis velocity
yd = q(5,:); % body fixed y-axis velocity
sd = q(6,:); % body yaw rate (psi_dot)
%xx = q(7,:); % global x position of car center of mass
%yy = q(8,:); % global y position of car center of mass 124
%Pass the constant values back through here
%Constants
m = 1724; % mass
Cd = 0.36; % coefficient of drag
A = 2.03; % car frontal area
g = 9.81; % acceleration due to gravity
sigma = 0.2; % grade
a = 1.51; % distance from center of mass to front axle
b = 1.26; % distance from center of mass to rear axle
c = 1.92; % track width;
w = 0.5*c; % half of the track width
H = 0.6; %height to center of gravity
L = a+b; % total length of the vehicle
mf = m * b / L; % mass on front axle
mr = m * a / L; % mass on rear axle
Cyr = 0.19*(mr)*g*(180/pi); % cornering stiffness rear tires (N/rad)
Cyf = 0.19*(mf)*g*(180/pi); % cornering stiffness front tires (N/rad)
rho = 1.225; % density of air
rtire = 0.29; % radius of tire (m)
mu = 0.8; % coefficient of friction
T21 = 500; % Torque to left rear tire (Nm)
T22 = 500; % Torque to right rear tire (Nm) 125

Izz = (1/12)*m*(L^2 + c^2) + m*(a-b)^2; %Moment of intertia
delta = 0.1; % Desired steering angle
% Tire slip angle
ad = xd - w*sd;
abs_ad = abs(ad);
alpha11 = 0;
if abs_ad > 0
```

```
alpha11 = atan((yd + a*sd)/ad) - delta;
end
alpha21 = 0;
if abs_ad > 0
alpha21 = atan((yd - b*sd)/ad);
end
af = xd + w*sd;
abs_af = abs(af);
alpha12 = 0;
if abs_af > 0
alpha12 = atan((yd + a*sd)/af) - delta; 126

end
alpha22 = 0;
if abs_af > 0
alpha22 = atan((yd - b*sd)/af);
end
axd = abs(xd);
% Tire forces
f11grade = 0;
if axd > 0
f11grade = -(mu*xd/axd)*(mu*H*m*g*cos(sigma) + b*m*g*cos(sigma))/(2*L);
end
f11x = -f11grade;
f11y = -Cyf*alpha11;
f21grade = 0;
if axd > 0
f21grade = -(mu*xd/axd)*(a*m*g*cos(sigma) - mu*H*m*g*cos(sigma))/(2*L);
end
f21x = -f21grade + T21/rtire;
f21y = -Cyr*alpha21; 127

f12grade = 0;
if axd > 0
f12grade = -(mu*xd/axd)*(mu*H*m*g*cos(sigma) + b*m*g*cos(sigma))/(2*L);
end
f12x = -f12grade;
f12y = -Cyf*alpha12;
f22grade = 0;
if axd > 0
f22grade = -(mu*xd/axd)*(a*m*g*cos(sigma) - mu*H*m*g*cos(sigma))/(2*L);
end
f22x = -f22grade + T22/rtire;
f22y = -Cyr*alpha22;
% Forces at center of mass
fdrag = 0.5*rho*Cd*A*xd*axd; % Longitudinal drag force
qdot(1,:) = xd;
qdot(2,:) = yd;
qdot(3,:) = sd;
qdot(4,:) = (f21x + f22x + f11x*cos(delta) + f12x*cos(delta) - sin(delta)*(f11y + f12y)- fdrag + sd*yd)/m; % Sum of
Forces in x-direction/m 128
qdot(5,:) = (-xd*sd + ( f11x*sin(delta) +f12x*sin(delta) + f11y*cos(delta) + f21y + f12y*cos(delta) + f22y )/m);
%Sum of Forces in y-direction/m
qdot(6,:) = (-f11x*cos(delta)*w + f11y*a*cos(delta) + f11x*a*sin(delta) + f11y*w*sin(delta) + f12x*cos(delta)*w +
f12y*a*cos(delta) + f12x*a*sin(delta) - f12y*w*sin(delta) - f21x*w - f21y*b - f22y*b + f22x*w)/Izz; %Sum of
Moments/I
qdot(7,:) = -yd*cos(s) - xd*sin(s); % global x position of car center of mass
qdot(8,:) = -yd*sin(s) + xd*cos(s); % global y position of car center of mass end 129
```